



Article

# The Flower-Shaped Co (II) and Cu (II) Phthalocyanine Polymers as Highly Efficient and Stable Catalysts for Chemical Fixation of CO<sub>2</sub> to Cyclic Carbonate

Yuyang Zhou, Shengyu Shao , Xiang Han, Baocheng Zhou , Yifeng Han, Xiaoping Dong \* and Sanchuan Yu

Key Laboratory of Surface & Interface Science of Polymer Materials of Zhejiang Province, School of Chemistry and Chemical Engineering, Zhejiang Sci-Tech University, Hangzhou 310018, China; zhouyuyang202202@163.com (Y.Z.); 15067755247@163.com (S.S.); hanxiang831@163.com (X.H.); hyflx@163.com (Y.H.); yuschn@163.com (S.Y.)

\* Correspondence: zhoubc1982@zstu.edu.cn (B.Z.); xpdong@zstu.edu.cn (X.D.)

**Abstract:** New flower-shaped metallophthalocyanine polymers (THB-4-M, M = Co, Cu) have been synthesized by using 1,3,5-Tri(4-hydroxyphenyl) benzene (THB) as rigid and contorted units to control the morphology under the solvothermal method. The polymers were characterized using FT-IR, UV-vis, SEM, TGA, and XPS. These polymers were applied as heterogeneous catalysts for the chemical fixation of carbon dioxide (CO<sub>2</sub>) to cyclic carbonates without solvent. The influence of reaction parameters and different metal centers on the catalytic performance were studied in detail. Under optimal conditions, the catalysts showed high conversion (49.9–99.0%), selectivity (over 85%), and reusability at ambient conditions (at 1 bar CO<sub>2</sub>).

**Keywords:** phthalocyanines polymers; carbon dioxide fixation; cyclic carbonate



**Citation:** Zhou, Y.; Shao, S.; Han, X.; Zhou, B.; Han, Y.; Dong, X.; Yu, S. The Flower-Shaped Co (II) and Cu (II) Phthalocyanine Polymers as Highly Efficient and Stable Catalysts for Chemical Fixation of CO<sub>2</sub> to Cyclic Carbonate. *C* **2024**, *10*, 74. <https://doi.org/10.3390/c10030074>

Academic Editors: Enrico Andreoli and Jorge Bedia

Received: 28 June 2024

Revised: 13 August 2024

Accepted: 17 August 2024

Published: 19 August 2024



**Copyright:** © 2024 by the authors. Licensee MDPI, Basel, Switzerland. This article is an open access article distributed under the terms and conditions of the Creative Commons Attribution (CC BY) license (<https://creativecommons.org/licenses/by/4.0/>).

## 1. Introduction

Metallophthalocyanines (MPcs) have been a theme of great interest in many areas, such as photovoltaic cells [1–3], non-linear optics [4,5], gas sensors [6,7], semiconductors [8,9], and so forth [10]. Metallophthalocyanines (MPcs) have four imino-isindoline rings with a conjugated 18 $\pi$ -electron system, and are highly stable synthetic tetrapyrrolic macrocycle compounds [11]. However, MPcs have shown insufficient electrocatalytic activity and poor catalytic performance due to their easy aggregation as they contain a planar-shaped structure [12]. To solve the aforementioned problem, many attempts have been made to prepare MPcs-loaded materials through the use of a nanomaterials, such as carbon nanotubes [13], graphene [14], Ag nanoparticle [15], and so on [16]. In addition, MPcs were suitable units of nanoporous materials due to their comprehensive application as catalysts and their electrocatalytic and non-linear optics characteristics. Covalent organic frameworks (COFs) [17], other nanomaterials [18–20], and metal–organic frameworks (MOFs) [21] have employed MPcs as their primary structural unit. Polymers of intrinsic microporosity (PIM) were also synthesized due to the inability of component macromolecules with a rigid and contorted structure, such as MPcs, have been developed over the past decade [22–29]. Such microporous polymers containing MPcs have attracted many researchers to study them as heterogeneous catalysts.

Furthermore, the strategy for introducing rigid and contorted units in polymeric catalyst held great attraction for many researchers. Those polymeric catalysts have shown excellent properties in terms of large specific surface area, high porosity, and strong acid resistance. McKeown et al. reported a new microporous MPcs network polymer synthesized from the interconnection of MPcs units through the rigid and contorted linkers to enhance of catalytic activity of MPcs [30]. Chen's group designed a 1,3,5-tris (1*H*-benzo[d]imidazol-2-yl) benzene-linked polymeric-sphere catalyst and showed high conversions and cyclic

organic carbonate yields at 298 K and 1 bar of CO<sub>2</sub> [31]. It was found that introduction of the rigid and contorted units can enhance the porosity of heterogeneous catalysts [30,31]. Specifically, 1,3,5-Tri(4-hydroxyphenyl) benzene (THB), as reported by many researchers, was applied, due to its excellent properties in terms of large specific surface area, high porosity, and strong acid resistance [32–36]. However, the network polymers reported were prepared by using high temperatures, a complicated line, and a special method.

In this study, we synthesized two microporous polymers containing MPCs that used 1,3,5-tri(4-hydroxyphenyl) benzene (THB) as the rigid and contorted units, and investigated the catalytic activity for CO<sub>2</sub> fixation (Figure 1).

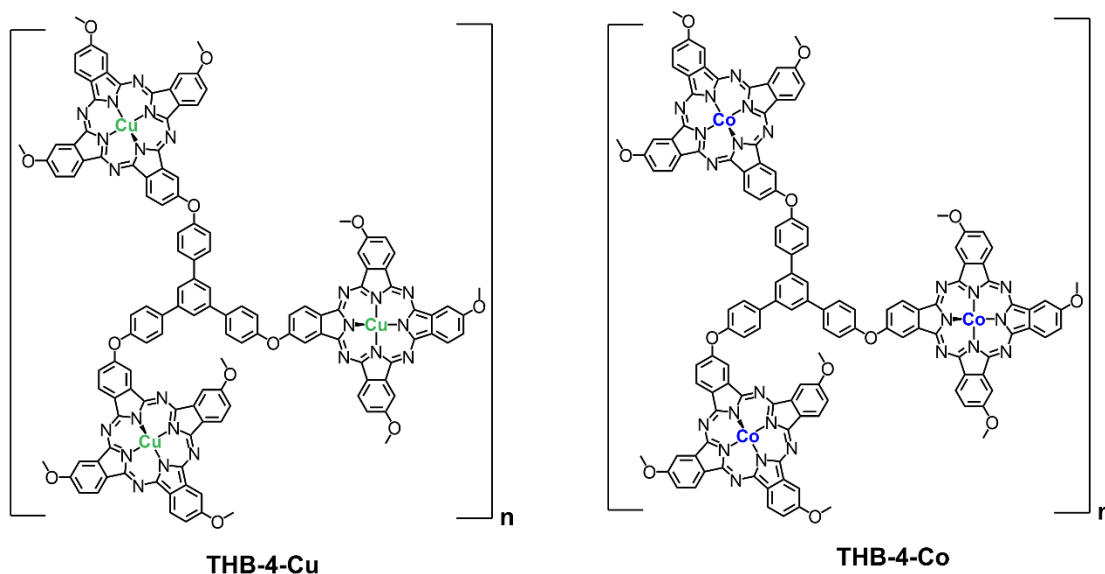


**Figure 1.** Chemical structure of MPCs network polymers THB-4-Cu and THB-4-Co.

## 2. Experimental

### 2.1. Materials

Silicon tetrachloride (SiCl<sub>4</sub>, 99.5%), 4-methoxyacetophenone (99.0%), pyridine hydrochloride (98.0%), 4-nitrophthalonitrile (98.0%), potassium carbonate (K<sub>2</sub>CO<sub>3</sub>, 98.0%), copric chloride dihydrate (CuCl<sub>2</sub>·2H<sub>2</sub>O, AR), cobalt chloride hexahydrate (CoCl<sub>2</sub>·6H<sub>2</sub>O, AR), and ethanol (>99.5%, Safe Dry) were acquired from Shanghai Macklin Biochemical Technology Co., Ltd. (China). Dimethylsulfoxide (DMSO, 99.5%), N, N-dimethylformamide (DMF, 99.5%), 1-hexanol (98.0%), 1,8-diazabicyclo [5.4.0] undec-7-ene (DBU, 99%), tetrabutylammonium bromide (TBAB, 99.0%), tetrabutylammonium chloride (TBAC, 99.0%), tetrabutylammonium iodide (TBAI, 99.0%), benzyltriethylammonium chloride (TEBAC, 98.0%), hexadecyl trimethyl ammonium bromide (CTAB, 99.0%), hexadecyl trimethyl ammonium chloride (CTAC, 99.0%), epichlorohydrin (ECH, 99.5%), styrene oxide (98.0%), cyclohexene oxide (98.0%), 1,2-epoxytetradecane (95.0%), and ethylene glycol diglycidyl ether (95.0%) were acquired from Shanghai Macklin Biochemical Co., Ltd. (Shanghai, China). Deionized water (18.2 MΩ cm) was employed throughout the experiments. The 1,3,5-tri(4-methoxyphenyl) benzene (TMOB) (Scheme S1) and 1,3,5-tri(4-hydroxyphenyl) benzene (THB) (Scheme S2) were obtained according to reference [37], respectively. Cobalt phthalocyanine and copper phthalocyanine were obtained according to reference [24].

### 2.2. Synthesis of Phthalonitrile

A reaction flask was charged with THB (2.16 g), 4-nitrophthalonitrile (3.12 g), anhydrous K<sub>2</sub>CO<sub>3</sub> (2.50 g), and dry DMSO (20.00 mL), and the reaction mixture was stirred at room temperature under a nitrogen atmosphere. Then, anhydrous K<sub>2</sub>CO<sub>3</sub> (1.25 g) was added in portions every 12 h. After 48 h, the precipitates were obtained after the resulting reaction mixture was poured into water (200.00 mL), and then filtered and further washed

with water, and the phthalonitrile was obtained (yield ca. 97%) and marked as THB-4, where "4" represents the 4-substituted. All the above products were confirmed by a series of characterization analyses (ESI\*).  $^1\text{H}$  NMR (400 MHz,  $\text{DMSO-}d_6$ ):  $\delta$  8.15 (d,  $J$  = 8.8 Hz, 3H), 8.08–8.02 (m, 6H), 7.99 (s, 3H), 7.86 (d,  $J$  = 2.6 Hz, 3H), 7.48 (dd,  $J$  = 8.8 Hz, 2.6 Hz, 3H), 7.38–7.31 (m, 6H).  $^{13}\text{C}$  NMR (75 MHz,  $\text{DMSO-}d_6$ , 293 K):  $\delta$  = 161.4, 154.2, 141.1, 137.9, 136.8, 129.9, 124.8, 123.3, 122.7, 121.2, 117.2, 116.4, 115.9, 108.3. HRMS (TOF-ES): calculated for ( $\text{C}_{48}\text{H}_{25}\text{N}_6\text{O}_3^+$ ),  $[\text{M}+\text{H}]^+$ , 733.1983, found 733.1981.

### 2.3. Synthesis of THB-4-M ( $M = \text{Co}, \text{Cu}$ )

Phthalonitrile (THB-4, 0.66 g),  $\text{CoCl}_2 \cdot 6\text{H}_2\text{O}$  (0.28 g), DBU (0.60 mL), and dry DMF (5.00 mL) were added to a beaker and stirred to form a solution. After dissolving, 55.00 mL 1-hexanol was added and stirred for 30 min. The mixture was transferred into a hydrothermal reactor, and the reaction temperature was maintained at  $160^\circ\text{C}$  for 24 h. Then, it was cooled to room temperature and washed with ethanol, DMF, acetone, deionized water, and ethanol by the Soxhlet extraction method in sequence. After that, the solid was dried thoroughly, and the product, a bluish-green solid (THB-4-Co), was obtained (0.40 g). THB-4-Cu was prepared following the same synthetic procedure as for THB-4-Co, except that  $\text{CoCl}_2 \cdot 6\text{H}_2\text{O}$  (0.28 g) was replaced by  $\text{CuCl}_2 \cdot 2\text{H}_2\text{O}$  (0.17 g) (Figure 2).

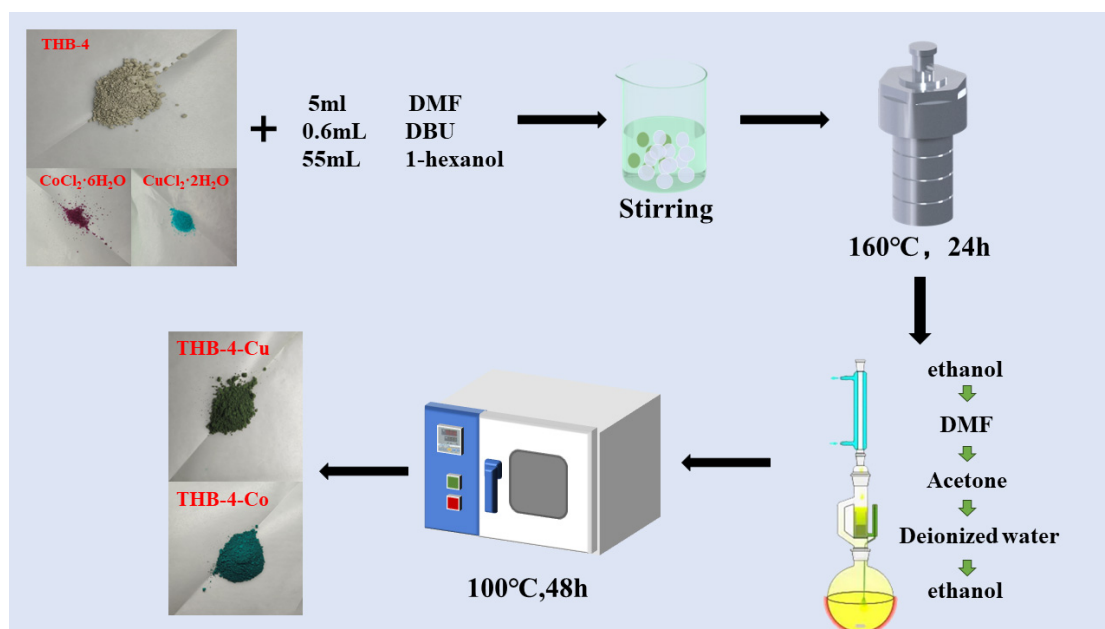


**Figure 2.** Schematic illustration for the synthesis of THB-4-Co and THB-4-Cu.

### 2.4. Characterizations

Various analytical techniques were employed to characterize the synthesized THB-4-Co and THB-4-Cu, such as Fourier transform infrared spectroscopy (FTIR), scanning electron microscopy (SEM), energy-dispersive X-ray spectrometry (EDS), and thermogravimetric analysis (TGA). An X-ray diffractometer (XRD, DX-2700) with  $\text{Cu-K}\alpha$  radiation ( $\lambda = 1.5418 \text{ \AA}$ ) was used to ensure the phase compositions and crystalline structure over a  $2\theta$  range of  $5\text{--}80^\circ$ . A field emission scanning electron microscope (FE-SEM, Hitachi SU-8100) equipped with an energy dispersive X-ray spectrometer (EDS) was employed to characterize the surface morphologies and micro/nanostructures of the THB-4-M. EDS was recorded at 15 kV and 15.0 mm sample distance at the Z-axis. All the samples were sputtered with platinum before observation. X-ray photoelectron spectra (XPS) were collected using multifunctional electron spectroscopy (Kratos, AXIS, Ultra, DLD) with  $\text{Al-K}\alpha$  radiation ( $h\nu = 1486.6 \text{ eV}$ ). The energy resolution during X-ray photoelectron spectra recording was 0.1 eV. All BE values were calibrated by using contaminant carbon on the catalyst

with C 1 s at 284.6 eV. Thermal stability analyses were conducted using a PerkinElmer Diamond TG-DTA instrument in a nitrogen atmosphere (15–850 °C; 20 °C/min). To obtain the specific surface area measurements of the THB-4-M, an ASAP-2020 Micromeritics was used in nitrogen physisorption at 77 K. The specific areas of the samples were determined by the Brunauer–Emmett–Teller (BET) procedure using nitrogen adsorption. The quantification of cobalt or copper loading on each sample was performed by inductively coupled plasma (ICP OES 730) emission spectrometry. The UV–VIS absorption spectra was gained using a UV–VIS spectrophotometer (Shimadzu UV-2600). To obtain the IR spectra (KBr pellets), the Nicolet Avatar 370 Fourier transform infrared spectra (FTIR) spectrometer was employed. The nuclear magnetic resonance (NMR) spectra of intermediate products were obtained using a Bruker AVANCE II 400NMR spectrometer. High-resolution mass spectra (HRMS) were recorded on a Waters TOFMS GCT Premier using ESI ionization. Elemental analysis was recorded by an Elementar UNICUBE using a thermal conductivity detector.

### 3. Results and Discussion

#### 3.1. Characterization of Network Polymers

First, the phthalonitrile monomer was synthesized from 4-nitrophthalonitrile and the twisting rings of 1,3,5-tri(4-hydroxyphenyl) benzene (THB) (Scheme S3). The monomer was completely confirmed by <sup>1</sup>H-NMR (Figure S1), <sup>13</sup>C-NMR (Figure S2). Then, we employed this as a component unit of the MPcs network polymers THB-4-Co and THB-4-Cu by coupling the condensation of 4-nitrophthalonitrile with a linker unit (THB) in the presence of metal salts ((CoCl<sub>2</sub>•6H<sub>2</sub>O) or (CuCl<sub>2</sub>•2H<sub>2</sub>O)) by the solvothermal method. Colorful polymers were obtained by the solvothermal reaction, washed, and subsequently purified by Soxhlet extraction (Figure 2).

Figure 3a shows the ultraviolet–visible (UV–VIS) DRS absorption of the complex (CoPc, THB-4-Co, CuPc, THB-4-Cu). The phthalocyanine network polymers showed typical electronic spectra with two absorption bands, which were similar to molecule phthalocyanines. THB-4-Co showed a split Q-band at 678 nm and 626 nm, whereas the CoPc exhibited a Q-band at 599 nm and 657 nm in CH<sub>2</sub>Cl<sub>2</sub> [38,39]; they were ascribed to the Q-band of monomeric and dimeric forms of MPcs. According to the curves, it was obviously above that the monomeric forms were more stabilized than the dimeric forms in CoPc/CH<sub>2</sub>Cl<sub>2</sub> solution; the dimeric forms showed more than the monomeric forms in the polymers, on the contrary. The same curve shape was also observed in the curves of CuPc and THB-4-Cu [28]. On account of being completely insoluble in normal solvent, the UV–VIS spectrum of CuPc in concentrated sulfuric acid revealed two bands: at 701 and 791 nm, which are characteristic of the dimeric and monomeric forms [29]. However, the as-prepared THB-4-Cu showed two bands: at 629 and 691 nm, which were red-shifted by 72 nm and 100 nm with that of CuPc in concentrated sulfuric acid, respectively. Furthermore, the emission maximum of polymer THB-4-Cu was red-shifted nearly 10 nm as compared with that of THB-4-Co, and it is well known that the difference is due to the central ion, as is typical for phthalocyanines. Additionally, a broadened and split Q-band was detected in both polymers due to the aggregation of MPcs, and the aggregate unit showed the high-energy band and the monomer showed the homologous low-energy band [28]. The emission maximum of polymer THB-4-Co was red-shifted nearly 20 nm as compared with that of CoPc, indicating that THB-4-Co had a narrower band gap than CoPc without regard to the solvent effect.

Table 1 summarizes the optical data of the complex (CoPc, THB-4-Co, CuPc, THB-4-Cu). IR peaks appeared in the range of 3068; 2856 cm<sup>-1</sup> were attributed to -C=C-H stretching vibrations of the aromatic groups of the phthalocyanines. The peaks at 1610, 1470, and 1390 cm<sup>-1</sup> belonged to C=C, C-N, and C=N stretching vibrations, respectively [40–42]. Figure 3b shows a similar tendency in both the polymers and the parent monomers. These FTIR spectroscopic data show that the objective product retained the most feature peaks of its corresponding unit. Thus, the above analysis results exactly verified the direct

heterogenization of THB-4-Co and THB-4-Cu polymers by the solvothermal reaction to produce very stable and heterogeneous porous polymeric materials.

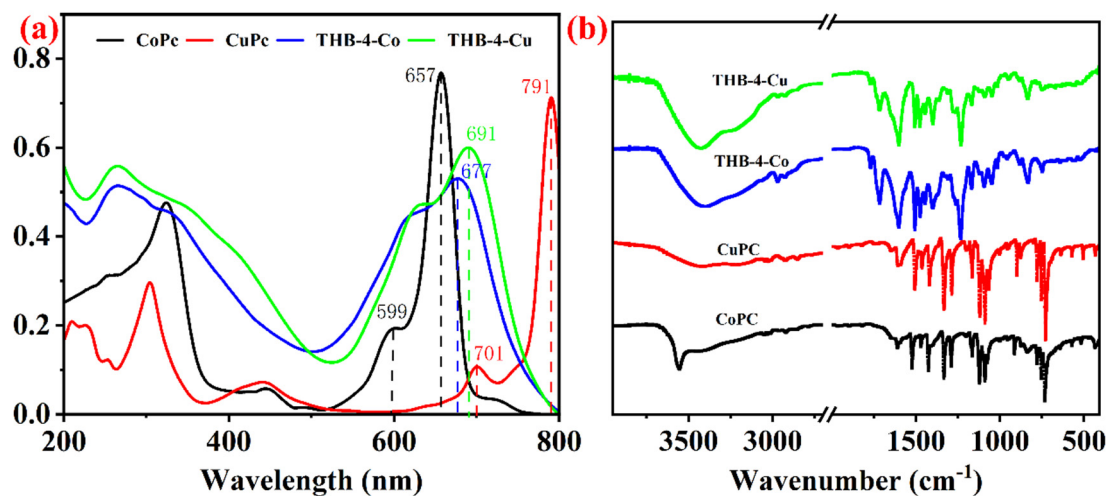


**Figure 3.** (a) UV-VIS diffuse reflectance spectra (DRS) of THB-4-Co, THB-4-Cu, CoPc, and CuPc. (b) FTIR of THB-4-Co, THB-4-Cu, CoPc, and CuPc.

**Table 1.** The optical data of THB-4-Co and THB-4-Cu.

Entry	MPcs	Absorption/nm	IR Peaks/cm <sup>-1</sup>
1	CoPc	599, 657 <sup>a</sup>	
2	THB-4-Co	626, 677	3068, 2856, 1610, 1470,
3	CuPc	701, 791 <sup>b</sup>	1390
4	THB-4-Cu	629, 691	

<sup>a</sup> Absorption spectra in CH<sub>2</sub>Cl<sub>2</sub> at a concentration 1.0 × 10<sup>-5</sup> mol/L. <sup>b</sup> Absorption spectra in concentrated sulfuric acid at a concentration of 1.0 × 10<sup>-5</sup> mol/L.

The thermal stabilities of these complexes (CoPc, THB-4-Co, CuPc, THB-4-Cu) were researched by thermogravimetric analysis to confirm the stability of the polymers. The TG curve of the as-prepared THB-4-M shows a similar trend with CoPc and CuPc, respectively. Additionally, that of the as-prepared THB-4-M was found to be thermally stable up to 400 °C, indicating possible outstanding thermal stability under harsh reaction conditions (Figure 4a inset figure, more details see Figure S8). It was shown that the weight loss of THB-4-Cu and THB-4-Co occurred at slight below 100 °C; we suspected that some solvent molecules were absorbed in the pores of the THB-4-M. The unit of THB was decomposed prior to the ring of phthalocyanine, according to the contrastive analysis. Notably, the weight loss of THB-4-Cu at 443 °C was only 14.5%, and the loss of THB-4-Co at 439 °C was 19.8%, and THB-4-Cu showed more thermostability than THB-4-Co.

Powder X-ray diffraction (PXRD) patterns were employed to assess the crystalline structure of these complexes (CoPc, THB-4-Co, CuPc, THB-4-Cu). As shown in Figure 4b, the diffraction peaks were affirmed as the crystalline structure of CoPc and CuPc [25]. Notably, the as-prepared polymers showed that a broad peak at 2θ = 19.42° corresponds to the construction of amorphous polymeric material and reveals a non-crystalline character [40–42] (Figure 4b). X-ray photoelectron spectroscopy (XPS) was employed to investigate the surface compositions of THB-4-Co and THB-4-Cu. The survey scans of XPS unambiguously verified the peaks attributed to carbon, nitrogen, and cobalt for THB-4-Co and copper for THB-4-Cu (Figure 5). As shown in Figure 5c, the Co (2p) XPS spectrum of THB-4-Co showed two deconvoluted peaks: at 797.0 and 781.2 eV, corresponding to Co (2p<sub>1/2</sub>) and Co (2p<sub>3/2</sub>), indicating that Co had coordinated with N to form Co-N<sub>x</sub> moieties [43–47]. In the case of THB-4-Cu, the presence of Cu (II) species was confirmed by the appearance of

two main peaks: at 953.3 and 933.1 eV, assigned to Cu ( $2p_{1/2}$ ) and Cu ( $2p_{3/2}$ ), as shown in Figure 5d. Additionally, the presence of C and N was also studied. Predictably, the C (1s) XPS spectrum of THB-4-Cu showed three deconvoluted peaks: at 284.8, 286.4, and 288.4 eV, attributed to C-C/C=C, C-N, and C-O. The N (1s) XPS spectrum of THB-4-Cu showed two peaks: at 398.5 and 400.1 eV, corresponding to the C-N and N-M (M = Cu, Co), as shown in Figure 6a,c [43–47]. The curves and the peaks were also exhibited in the XPS spectrum of THB-4-Co, as shown in Figure 6b,d [43–47]. Therefore, the Co(2p) XPS analysis of THB-4-Co and the Cu(2p) XPS analysis of THB-4-Cu confirmed successful as-prepared THB-4-M polymers.

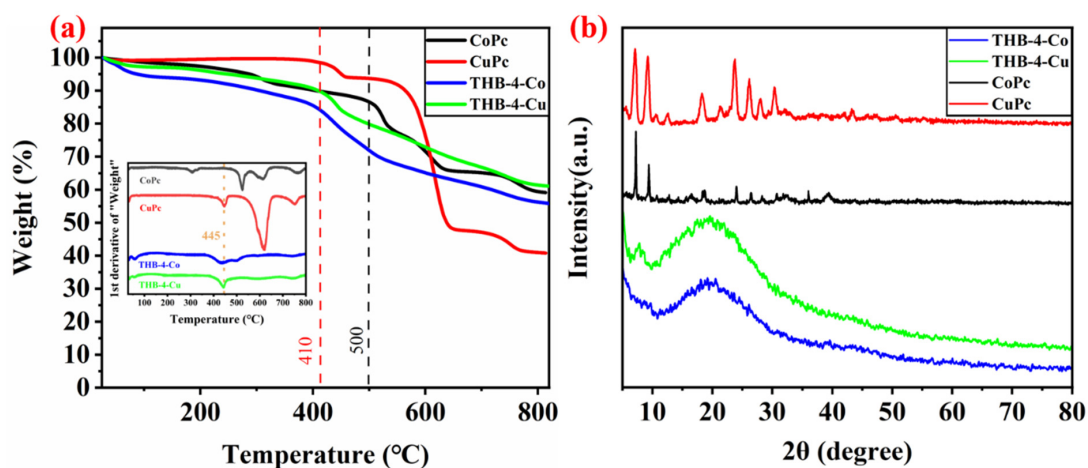


**Figure 4.** (a) Thermogravimetric analysis (TGA) of the THB-4-M. (b) The XRD patterns of the THB-4-M.

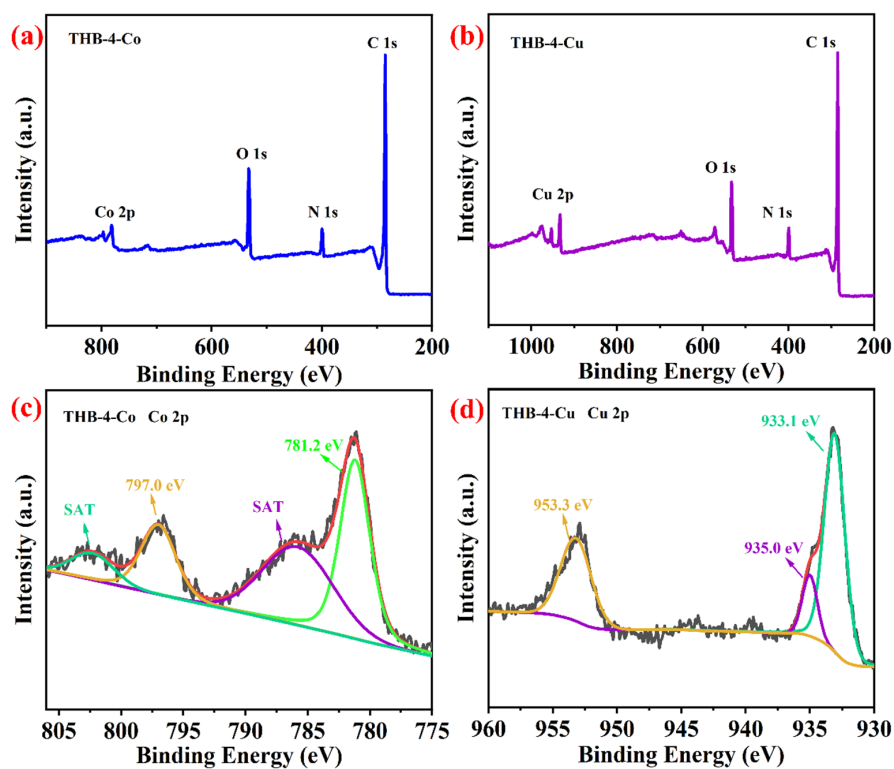


**Figure 5.** (a) XPS scan spectra for THB-4-Co; (b) XPS spectra for THB-4-Cu; (c) Co(2p) XPS spectra of THB-4-Co; and (d) Cu(2p) XPS spectra of THB-4-Cu.

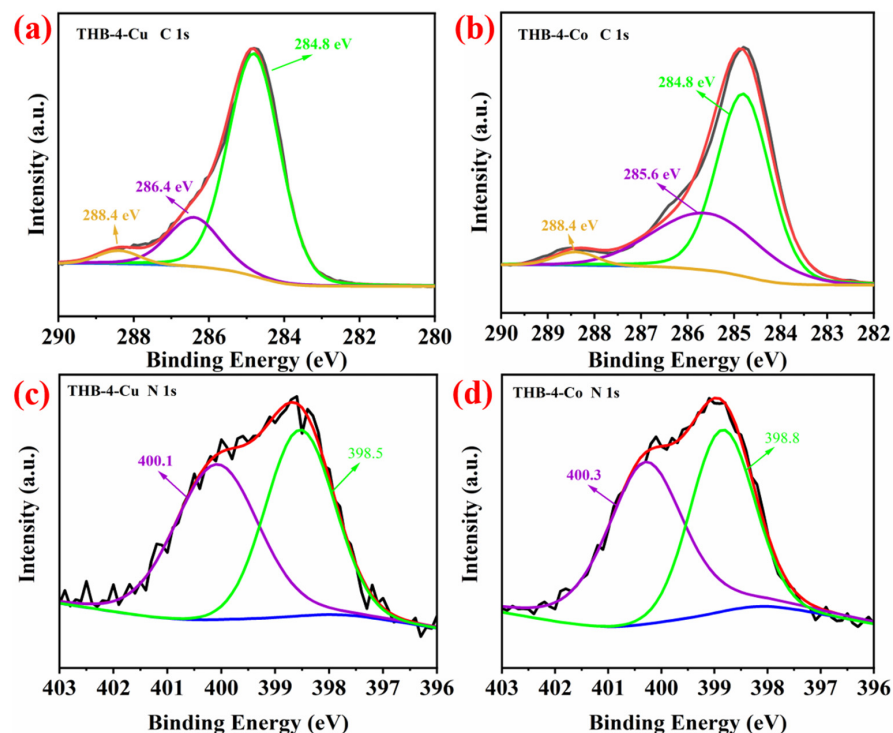


**Figure 6.** (a) C(1s) XPS spectra of THB-4-Cu; (b) C(1s) XPS spectra of THB-4-Co; (c) N(1s) XPS spectra of THB-4-Cu; and (d) N(1s) XPS spectra of THB-4-Co.

To more deeply comprehend the physical structure of the as-prepared THB-4-M polymers,  $N_2$ -adsorption–desorption,  $CO_2$ -adsorption–desorption, and scanning electron microscopy (SEM) were employed. The  $N_2$  adsorption–desorption isotherm was recorded at 77 K to investigate the porosities of the THB-4-Co and THB-4-Cu. It was found that the THB-4-M polymers showed a typical type-IV isotherm (Figure 7a,c) with a surface area of material of  $71.14 \text{ m}^2 \cdot \text{g}^{-1}$  and  $114.25 \text{ m}^2 \cdot \text{g}^{-1}$  (Table 2). The as-prepared materials were capable of adsorbing obvious amounts of  $CO_2$  molecules under the ambient conditions. The corresponding test had been measured to gain the  $CO_2$  adsorption isotherms (Figure 7b,d). The  $CO_2$  adsorption isotherms were carefully tested up to 760 mm Hg. As shown in Table 2, the THB-4-Co showed the uptake capacities  $24.14$  and  $14.17 \text{ cm}^3 \cdot \text{g}^{-1}$  at 273 and 298 K; the THB-4-Cu showed the uptake capacities  $25.40$  and  $9.68 \text{ cm}^3 \cdot \text{g}^{-1}$  at 273 and 298 K, respectively. In this regard, the uptake capacities of THB-4-Co were superior to the uptake capacities of THB-4-Cu at 298 K.

The morphology of CoPc, CuPc, and THB-4-M is displayed in SEM images (Figure 8 and Figure S9). The morphology of CoPc and CuPc were shown as the normal crystalline form, consistent with the performance of the XRD spectra. The morphology of THB-4-M was flower-shaped, with the size of each petal estimated to be ca. 60–80 nm. The morphology of THB-4-Cu was shown to be smoother than that of THB-4-Co (Figure 8b,e). Subsequently, SEM-EDS and SEM-mapping analysis confirmed the complexation of Co and Cu into the polymeric frameworks along with other elements, such as C, N, and O. Therefore, all elements were distributed uniformly over the as-prepared polymers (Figure 9 and Figure S10), and the elemental analysis of the THB-4-M polymers is shown in Table S1. The found data might not be relevant or up to the calculated data because of the impurity of the polymers.

**Table 2.** Characterization data of THB-4-M polymers.

Entry	MPcs	$S_{\text{BET}}$ ( $\text{m}^2 \cdot \text{g}^{-1}$ )	$V_{\text{pore}}$ ( $\text{cm}^3 \cdot \text{g}^{-1}$ )	$D_{\text{pore}}$ (nm)	$CO_2$ Capacities (273 K, $\text{cm}^3 \cdot \text{g}^{-1}$ )	$CO_2$ Capacities (298 K, $\text{cm}^3 \cdot \text{g}^{-1}$ )	ICP
1	THB-4-Co	71.14	0.36	24.07	24.14	14.17	7.73
2	THB-4-Cu	114.25	0.25	19.71	25.40	9.68	8.52

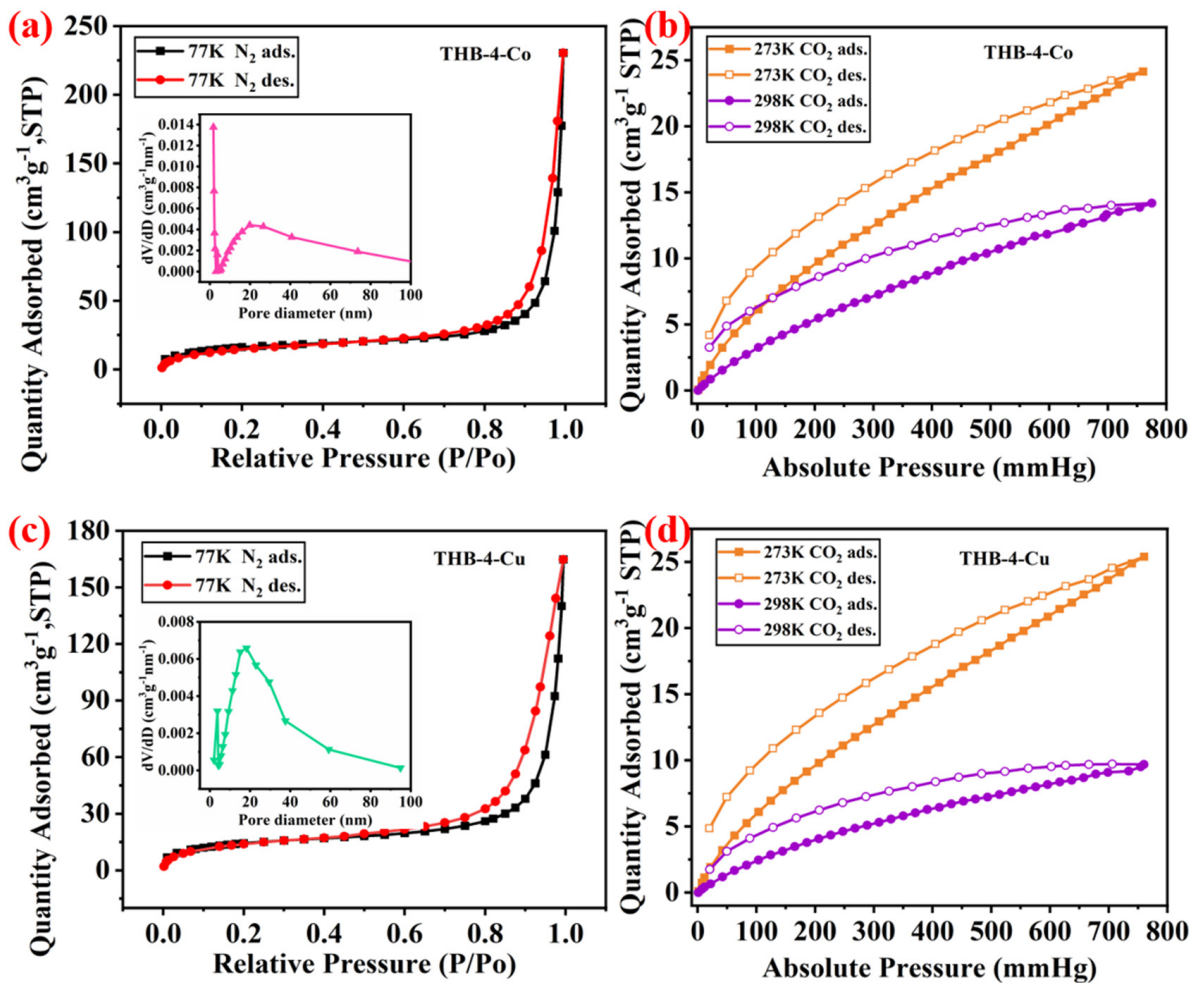


**Figure 7.** (a)  $N_2$  adsorption–desorption isotherms of THB-4-Co. (b)  $CO_2$  uptake isotherms of THB-4-Co at both 273 K and 298 K. (c)  $N_2$  adsorption–desorption isotherms of THB-4-Cu. (d)  $CO_2$  uptake isotherms of THB-4-Cu at both 273 K and 298 K.

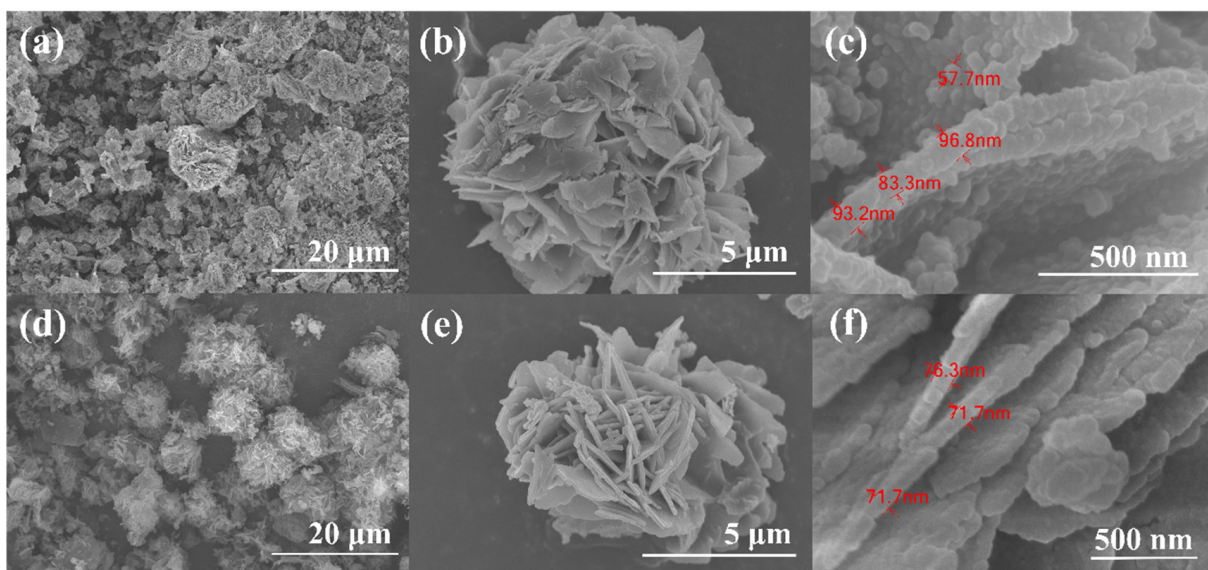


**Figure 8.** SEM images of as-prepared polymers with different ions: (a–c) was THB-4-Co and (d–f) was THB-4-Cu.

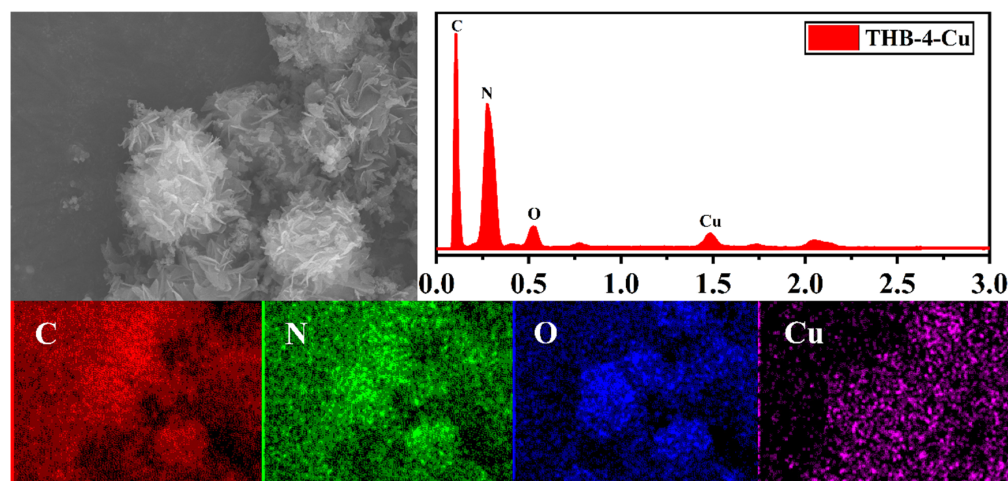
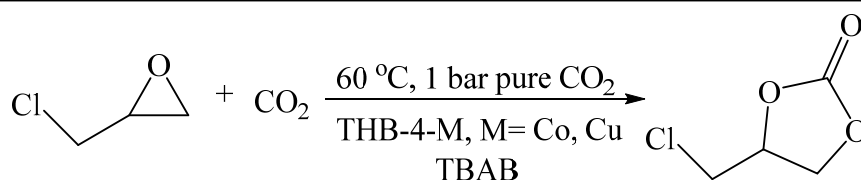


**Figure 9.** EDS and mapping of THB-4-Cu.

### 3.2. Cycloaddition of CO<sub>2</sub> to Cyclic Carbonate

As mentioned in the introduction, the new flower-shaped catalysts were employed in the cycloaddition of CO<sub>2</sub> to epoxides. As shown in Table 3, we applied these network polymers as catalysts in the synthesis of cyclic carbonates. The cycloaddition of pure CO<sub>2</sub> (1 bar) with epichlorohydrin (ECH) as substrate and tetrabutylammonium bromide (TBAB) as co-catalyst at certain temperatures in solvent-free conditions was selected as a model reaction to start our research. Surprisingly, both THB-4-Cu and THB-4-Co showed excellent conversion under the above reaction conditions, and exhibited better TON than certain catalysts that contained Cu ion and Co ion.

**Table 3.** The cycloaddition of CO<sub>2</sub> with ECH catalyzed by THB-4-M under solvent-free conditions.



Entry	Catalysts	P CO <sub>2</sub> (bar)	T (°C)	t (h)	Conv. (%)	TON <sup>(a)</sup>	Ref.
1	Co/POP-TPP/TBAB	1	29	24	95.6	442	[48]
2	CoPc/g-C <sub>3</sub> N <sub>4</sub>	30	130	24	97.6	296	[40]
3	CoPc-NDs/TBAB	1	25	24	88.0	1708	[49]
4	Co-CMP/TBAB	3	100	1	98.1	201	[50]
5	FTPFs-Cu-Nb-Ni/TBAB	1	r.t.	48	93.0	186	[51]
6	CuPc@CS/TBAB	1	80	4.5	95.0	270	[29]
7	FJI-H7(Cu)/TBAB	1	25	60	66.5	332.5	[29]
8	MMPF-9(Cu)/TBAB	1	25	48	87.4	NM <sup>(b)</sup>	[52]
9	MMCF-2(Cu)/TBAB	1	r.t.	48	88.5	NM	[53]
10	CoPc/TBAB	/ <sup>(c)</sup>	140	5	5.1	NM	[54]
11	THB-4-Co/TBAB	1	60	24	90.3	674	This work <sup>(d)</sup>
12	THB-4-Cu/TBAB	1	60	24	91.6	676	This work

<sup>(a)</sup> Turn-over number (mol substrate converted/mol catalysts based on Cu); <sup>(b)</sup> NM: not mentioned; <sup>(c)</sup> CO<sub>2</sub> 360 mmol; <sup>(d)</sup> Reaction conditions: 1.00 g epichlorohydrin (ECH), 10 mg THB-4-M (0.013 mmol MPc), and 50 mg TBAB (the mass ratio of catalyst: co-catalyst = 1:5) were added to a Schlenk tube with a CO<sub>2</sub> balloon (1 bar pure CO<sub>2</sub>) under solvent-free conditions.

First, reaction conditions such as the amount of co-catalyst, temperature, and reaction time were screened using epichlorohydrin as the substrate (Table 4). Typically, 1.00 g of epichlorohydrin (ECH), 10 mg of catalyst (THB-4-M, 0.013 mmol MPc), and 50 mg TBAB (the mass ratio of catalyst and co-catalyst was 1:5) were added to a Schlenk tube with a

CO<sub>2</sub> balloon (1 bar pure CO<sub>2</sub>) under solvent-free conditions. First, the tube was placed under a vacuum and purged three times, and the pressure of CO<sub>2</sub> was set by the CO<sub>2</sub> balloon (1 bar pure CO<sub>2</sub>). The mixture was stirred at the given temperature and time. Similar to the literature [29], TBAB showed low catalytic performance, and the conversion was only 47.3% in our system, but higher than the review. CuPc and CoPc exhibited no catalytic performance and were also confirmed in this system. Remarkably, in our case, the conversion and selectivity of ECH were determined by <sup>1</sup>H NMR spectra analysis using 1,3,5-trimethoxybenzene as an internal standard (Figure S11) [55,56].

Quaternary ammonium halides were employed as a co-catalyst in the commercial synthetic process for cyclic carbonates [57]. Table 4 shows that the alkyl group and the counter anion of the quaternary ammonium salt significantly affect the catalytic activity. With regard to different alkyl groups, catalytic activity increased in the following order: TBA<sup>+</sup> < CTA<sup>+</sup> < TEBA<sup>+</sup> (Table 4, entry 3–5). As expected, Br<sup>−</sup> showed the best selectivity and highest conversion among the different halide ions [33,58–60] (Table 4, entry 1–3). The amount of co-catalyst in the catalytic system also affected the conversion and selectivity of chloropropene carbonate from CO<sub>2</sub> and ECH (Table 4, entry 12–14). The conversion and selectivity of ECH increased along with the amount of TBAB. Furthermore, we studied the effect of the reaction time (Table 4, entry 7–10). It was found that the conversion of the ECH increased obviously by the increase in the reaction time. Unfortunately, the selectivity of the corresponding carbonate decreased after 48 h. Notably, high temperatures accelerated both the conversion and selectivity of ECH (Table 4, entry 7–11). In addition, it was found that both the conversion and selectivity increased obviously by an increase in the mass fraction of TBAB in the mass ratio of THB-4-Cu/TBAB (Table 4, entry 12–14).

Under the optimized reaction parameters, we further expanded this catalytic system to synthesis of various cyclic carbonates using THB-4-M as the catalyst (Tables 4 and S3, entry 15–19). All the provided substrates under the optimized reaction conditions provided medium to good yields and selectivity towards the cyclic carbonates. Unfortunately, the steric effect also caused lower conversion and selectivity, similar to the literature [19,25,37] (Table 4, entry 16). For 1,2-epoxytetradecane, the corresponding carbonate was obtained in a low yield of 65.7% and 62.6% (Table 4 and Table S3, entry 18), presumably due to the flexibility of the aliphatic chain of the tetradecane oxide. It is important to note that the THB-4-Co exhibited the same catalytic performance and selectivity (Table S3).

**Table 4.** Catalytic performance of THB-4-Cu and various epoxides in the thermal cycloaddition of CO<sub>2</sub> to epoxides.

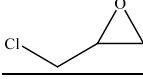
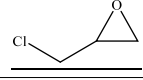
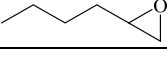
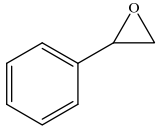
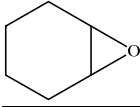
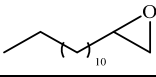
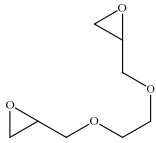
Entry	Epoxide	Co-Cat <sup>(a)</sup>	T (°C)	t (h)	Conv. (%) <sup>(b)</sup>	Selec. (%) <sup>(b)</sup>	TON <sup>(c)</sup>
1		TBAB	60	24	90.3	90.5	674
2		TBAI			89.9	95.6	709
3		TBAC			78.7	73.3	476
4		TEBAC			88.0	70.3	510
5		CTAC			79.0	69.2	451
6		CTAB			94.9	81.2	635
7		TBAB	60	6	69.5	69.3	397
8				12	83.9	90.5	626
9				24	90.3	90.5	674
10				48	98.0	89.1	720
11				12	99.0	92.6	756
12		TBAB 50 mg	60	24	90.3	90.5	674
13		TBAB 30 mg			83.6	87.3	601
14		TBAB 10 mg			73.6	78.4	475
15		TBAB	90	24	82.4	90.3	613

Table 4. Cont.

Entry	Epoxide	Co-Cat <sup>(a)</sup>	T (°C)	t (h)	Conv. (%) <sup>(b)</sup>	Selec. (%) <sup>(b)</sup>	TON <sup>(c)</sup>
16		TBAB	90	24	90.1	92.6	697
17		TBAB	90	24	49.9	35.5	146
18		TBAB	90	24	65.7	88.4	239
19		TBAB	60	24	69.7	50.4	142

<sup>(a)</sup> Reaction conditions: 1.00 g epichlorohydrin (ECH), 10 mg THB-4-Cu (0.013 mmol CuPc), and 50 mg TBAB (the mass ratio of catalyst: co-catalyst = 1:5) were added to a Schlenk tube with CO<sub>2</sub> balloon (1 bar pure CO<sub>2</sub>) under solvent-free conditions; <sup>(b)</sup> Conversion and selectivity determined by <sup>1</sup>H NMR spectra analysis using 1,3,5-trimethoxybenzene as an internal standard; <sup>(c)</sup> Turn-over number (mol substrate converted/mol catalysts based on Cu).

### 3.3. Catalyst Recycling Performance

The most important performance for an ideal heterogeneous catalyst was the reusability and stability of the catalysts. A three-cycle test was performed to probe the reusability of THB-4-M in the cycloaddition reactions (ESI<sup>\*</sup>). Additionally, the change of morphology obtained from SEM was also evaluated for the stability of the catalysts. Figure 10 shows the conversion and selectivity of ECH catalyzed by THB-4-M. In contrast, the THB-4-Co and THB-4-Cu showed more stability by analyzing the conversion and the morphology of the catalyst (Figure 10b,c). Unfortunately, the conversion of ECH catalyzed by THB-4-Cu reduced from 90.3% to 86.9%, presumably due to the reduction of the surface area and the CO<sub>2</sub> uptake capacities (ESI<sup>\*</sup>). The content of cobalt or copper loading was also an important influencing factor, causing the variation of the conversion and selectivity of ECH. Interestingly, the selectivity of ECH was enhanced from 90.5% to 97.3%. On the contrary, the conversion and selectivity of ECH catalyzed by THB-4-Co reduced observably.

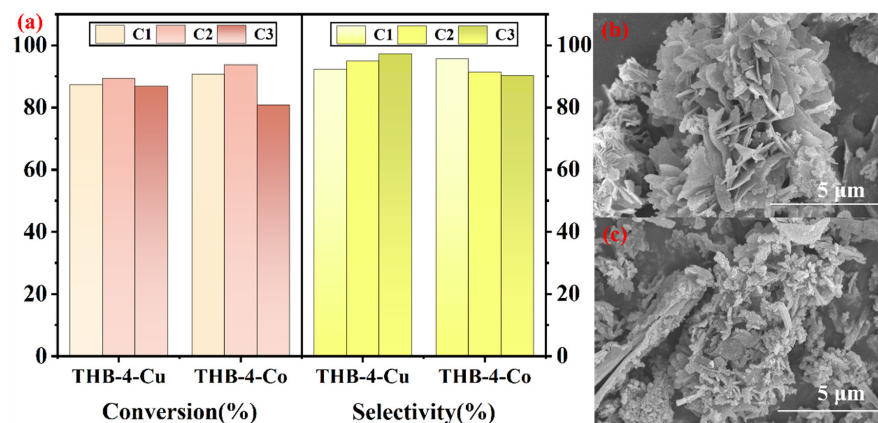
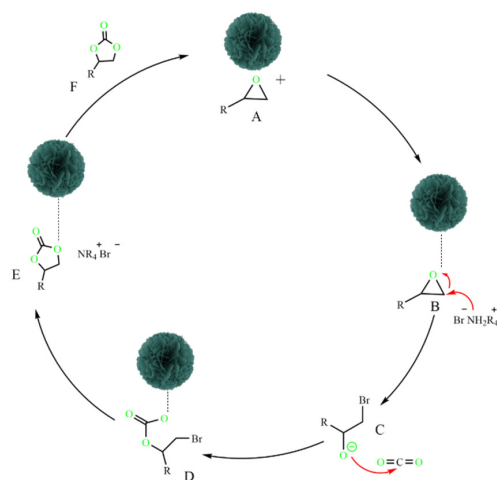


Figure 10. (a) The conversion and selectivity catalyzed by THB-4-M; (b) SEM images of THB-4-Cu after three recycling cycles; (c) SEM images of THB-4-Co after three recycling cycles.

### 3.4. Possible Reaction Mechanism

Based on previous reports [33,57], a plausible mechanism is proposed for the reaction of epoxide and CO<sub>2</sub> into cyclic carbonate catalyzed by THB-4-M in the presence of TBAB as a co-catalyst (Scheme 1). At first, CO<sub>2</sub> molecules were adsorbed by THB-4-M (M = Cu, Co) and the coupling reaction by coordination of MPc (M = Cu, Co) as a Lewis acidic site with the O atom of the ECH to form a metal alkoxide intermediate (B). The coordination between the MPc (M = Cu, Co) and ECH was shown as the crucial factor [37]. In the second step, halogen ions, such as Br<sup>-</sup>, attacked the less-hindered carbon atom of ECH, and the ring of ECH opened. Then, CO<sub>2</sub> molecules, which had been adsorbed, interacted with the oxygen anion of the opened epoxy ring to form an intermediate (D). In the end, the formation of cyclic carbonate and regeneration of catalyst THB-4-M were obtained along with the departure of Br<sup>-</sup>.



**Scheme 1.** Proposed mechanism for the coupling of CO<sub>2</sub> and ECH promoted by THB-4-M (M = Cu, Co).

## 4. Conclusions

In summary, new flower-like phthalocyanine polymers have been successfully synthesized by introducing 1,3,5-tri(4-hydroxyphenyl) benzene (THB) as the rigid and contorted units. Due to their porosity and excellent CO<sub>2</sub> capacities, the THB-4-M showed very promising catalytic activities with 146–756 TON in the conversion of CO<sub>2</sub> into cyclic carbonates. In addition, the THB-4-M showed high catalytic performance and excellent selectivity toward the cycloaddition reaction under mild conditions. Under optimal reaction conditions, ECH showed 99.0% conversion and 92.6% selectivity. The catalyst THB-4-M was readily separated and effectively recycled for up to three cycles. More importantly, the high stability and reusability of the catalyst benefitted from the flower-like structure of THB-4-M. According to the research results, this opens new ways of thinking about designing more efficient heterogeneous catalysts and fixing CO<sub>2</sub> by chemical methods under mild conditions.

**Supplementary Materials:** The following supporting information can be downloaded at: <https://www.mdpi.com/article/10.3390/c10030074/s1>.

**Author Contributions:** Investigation, methodology, writing—original draft, Y.Z.; methodology, validation, formal analysis, S.S.; methodology, validation, formal analysis, X.H.; conceptualization, investigation, methodology, writing—original draft, writing—review and editing, B.Z.; supervision, writing—review and editing, Y.H.; supervision, formal analysis, writing—review and editing, X.D.; supervision, formal analysis, writing—review and editing, S.Y. All authors have read and agreed to the published version of the manuscript.

**Funding:** We are grateful for financial support from the National Key Research and Development Program of China (2017YFE0127400), Zhejiang Special Support Program for High-Level Talents (No.

2023R5229), the Natural Science Foundation of China (51908491), and the Zhejiang Provincial Natural Science Foundation of China (LY20B070001).

**Data Availability Statement:** The data presented in this study are available on request from the corresponding author.

**Conflicts of Interest:** The authors declare no conflicts of interest.

## References

1. Zhang, S.H.; Tian, C.; Jiang, X.W.; Xu, X.; Zhao, H.T.; Sun, J.Y.; Zhang, L.F.; Cheng, Z.P. Synthesis of water-soluble NIR macro-photocatalysts from polymerizable zinc phthalocyanine. *Eur. Polym. J.* **2023**, *196*, 112313. [[CrossRef](#)]
2. Xu, R.; Li, B.L.; Ding, J.L.; Li, W.; Zhang, Y.H. Donor–acceptor conjugates-functionalized aluminum phthalocyanines: Photophysical and nonlinear optical properties. *Eur. Polym. J.* **2020**, *134*, 109813. [[CrossRef](#)]
3. Wöhrle, D.; Kreienhoop, L.; Schnurpfeil, G.; Elbe, J.; Tennigkeit, B.; Hiller, S.; Schlettwein, D. Investigations of n/p-junction photovoltaic cells of perylenetetracarboxylic acid diimides and phthalocyanine. *J. Mater. Chem.* **1995**, *5*, 1819–1829. [[CrossRef](#)]
4. Chen, X.N.; Zhang, J.L.; Wei, W.W.; Jiang, Z.H.; Zhang, Y.H. Synthesis and third-order optical nonlinearities of hyperbranched metal phthalocyanines. *Eur. Polym. J.* **2014**, *53*, 58–64. [[CrossRef](#)]
5. Diaz Garcia, M.A.; Ledoux, I.; Duro, J.A.; Torres, T.; Agullo-Lopez, F.; Zyss, J. Third-order nonlinear optical properties of soluble octasubstituted metallophthalocyanines. *J. Phys. Chem.* **1994**, *98*, 8761–8764. [[CrossRef](#)]
6. Li, B.W.; Wei, P.R.; Leon, A.D.; Frey, T.; Pentzer, E. Polymer composites with photo-responsive phthalocyanine for patterning in color and fluorescence. *Eur. Polym. J.* **2017**, *89*, 399–405. [[CrossRef](#)]
7. Wright, J.D.; Roisin, P.; Rigby, G.P. Crowned and liquid-crystalline phthalocyanines as gas-sensor materials. *Sens. Actuators B* **1993**, *13*, 276–280. [[CrossRef](#)]
8. Huai, M.M.; Yin, Z.L.; Wei, F.Y.; Wang, G.W.; Xiao, L.; Lu, J.T.; Zhuang, L. Electrochemical CO<sub>2</sub> reduction on heterogeneous cobalt phthalocyanine catalysts with different carbon supports. *Chem. Phys. Lett.* **2020**, *754*, 137655. [[CrossRef](#)]
9. Zhou, R.; Josse, F.; Gopel, W.; Ozturk, Z.Z.; Bekaroglu, O. Phthalocyanines as Sensitive Materials for Chemical Sensors. *Appl. Organomet. Chem.* **1996**, *10*, 557–577. [[CrossRef](#)]
10. Mevlüde, C.; Tebello, N. Synthesis, characterization, and photophysical properties of novel ball-type dinuclear and mononuclear containing four 1,1'-binaphthyl-8,8'-diol bridged metallophthalocyanines with long triplet state lifetimes. *Dalton Trans.* **2011**, *40*, 5285–5290.
11. Al-Raqa, S.Y.; Ghanem, B.S.; Kaya, E.N.; Durmus, M.; El-Khouly, M.E. Symmetrical phthalocyanine bearing four triptycene moieties: Synthesis, photophysical and singlet oxygen generation. *J. Porphyr. Phthalocyanines* **2019**, *23*, 990–1000. [[CrossRef](#)]
12. Li, T.F.; Peng, Y.X.; Li, K.; Zhang, R.; Zheng, L.R.; Xia, D.G.; Zuo, X. Enhanced activity and stability of binuclear iron (III) phthalocyanine on graphene nanosheets for electrocatalytic oxygen reduction in acid. *J. Power Sources* **2015**, *293*, 511–518. [[CrossRef](#)]
13. Zhang, X.; Wu, Z.S.; Zhang, X.; Li, L.W.; Li, Y.Y.; Xu, H.M.; Li, X.X.; Yu, X.L.; Zhang, Z.S.; Liang, Y.Y.; et al. Highly selective and active CO<sub>2</sub> reduction electro-catalysts based on cobalt phthalocyanine/carbon nanotube hybrid structures. *Nat. Commun.* **2017**, *8*, 14675. [[CrossRef](#)] [[PubMed](#)]
14. Guo, J.; Yan, X.M.; Liu, Q.; Li, Q.; Xu, X.; Kang, L.T.; Cao, Z.M.; Chai, G.L.; Chen, J.; Wang, Y.B.; et al. The synthesis and synergistic catalysis of iron phthalocyanine and its graphene-based axial complex for enhanced oxygen reduction. *Nano Energy* **2018**, *46*, 347–355. [[CrossRef](#)]
15. Costa, Í.A.; Maciel, A.P.; Sales, M.J.A.; Rivera, L.M.R.; Soler, M.A.G.; Pereira-da-Silva, M.A.; Moreira, S.G.C.; Paterno, L.G. Photocatalytic Method for the Simultaneous Synthesis and Immobilization of Ag Nanoparticles onto Solid Substrates. *J. Phys. Chem. C* **2018**, *122*, 24110–24119. [[CrossRef](#)]
16. Liu, D.; Long, Y.T. Superior catalytic activity of electrochemically reduced graphene oxide supported iron phthalocyanines toward oxygen reduction reaction. *ACS Appl. Mater. Interfaces* **2015**, *7*, 24063–24068. [[CrossRef](#)] [[PubMed](#)]
17. Ding, X.S.; Guo, J.; Feng, X.A.; Honsho, Y.; Guo, J.D.; Seki, S.; Maitarad, P.; Saeki, A.; Nagase, S.; Jiang, D.L. Synthesis of Metallophthalocyanine Covalent Organic Frameworks That Exhibit High Carrier Mobility and Photoconductivity. *Angew. Chem. Int. Ed.* **2011**, *50*, 1289–1293. [[CrossRef](#)]
18. Bezzu, C.G.; Warren, J.E.; Helliwell, M.; Allan, D.R.; McKeown, N.B. Heme-like coordination chemistry within nanoporous molecular crystals. *Science* **2010**, *327*, 1627–1630. [[CrossRef](#)]
19. Li, J.T.; Guo, L.M.; Shi, J.L. Stepwise in situ synthesis and characterization of metallophthalocyanines@mesoporous matrix SBA-15 composites. *Phys. Chem. Chem. Phys.* **2010**, *12*, 5109–5114. [[CrossRef](#)]
20. Lopez-Duarte, I.; Dieu, L.Q.; Dolamic, I.; Martinez-Diaz, M.V.; Torres, T.; Calzaferri, G.; Bruhwiler, D. On the significance of the anchoring group in the design of antenna materials based on phthalocyanine stopcocks and zeolite L. *Chem. A Eur. J.* **2011**, *17*, 1855–1862. [[CrossRef](#)]
21. Zalomaeva, O.V.; Kovalenko, K.A.; Chesalov, Y.A.; Mel'gunov, M.S.; Zaikovskii, V.I.; Kaichev, V.V.; Sorokin, A.B.; Kholdeeva, O.A.; Fedin, V.P. Iron tetrasulfophthalocyanine immobilized on metal organic framework MIL-101: Synthesis, characterization and catalytic properties. *Dalton Trans.* **2011**, *40*, 1441–1444. [[CrossRef](#)]

22. McKeown, N.B.; Budd, P.M. Exploitation of Intrinsic Microporosity in Polymer-Based Materials. *Macromolecules* **2010**, *43*, 5163–5176. [[CrossRef](#)]
23. McKeown, N.B.; Budd, P.M. Polymers of Intrinsic Microporosity (PIMs): Organic Materials for Membrane Separations, Heterogeneous Catalysis and Hydrogen Storage. *ChemInform* **2006**, *35*, 675–683.
24. McKeown, N.B.; Makhseed, S.; Budd, P.M. Phthalocyanine-based nanoporous network polymers. *Chem. Commun.* **2002**, *23*, 2780–2781. [[CrossRef](#)]
25. Maffei, A.V.; Budd, P.M.; McKeown, N.B. Adsorption studies of a microporous phthalocyanine network polymer. *Langmuir: ACS J. Surf. Colloids* **2006**, *22*, 4225–4229. [[CrossRef](#)]
26. Makhseed, S.; Al-Kharafi, F.; Samuel, J.; Ateya, B. Catalytic oxidation of sulphide ions using a novel microporous cobalt phthalocyanine network polymer in aqueous solution. *Catal. Commun.* **2009**, *10*, 1284–1287. [[CrossRef](#)]
27. Mackintosh, H.J.; Budd, P.M.; McKeown, N.B. Catalysis by microporous phthalocyanine and porphyrin network polymers. *J. Mater. Chem.* **2008**, *18*, 573–578. [[CrossRef](#)]
28. Tamura, R.; Kawata, T.; Hattori, Y.; Kobayashi, N.; Kimura, M. Catalytic oxidation of thiols within cavities of phthalocyanine network polymers. *Macromolecules* **2017**, *50*, 7978–7983. [[CrossRef](#)]
29. Boroujeni, M.B.; Laeini, M.S.; Nazeri, M.T.; Shaabani, A. A novel and green in situ strategy for the synthesis of metallophthalocyanines on chitosan and investigation their catalytic activity in the CO<sub>2</sub> fixation. *Catal. Lett.* **2019**, *149*, 2089–2097. [[CrossRef](#)]
30. Hashem, M.; Bezzu, C.G.; Kariuki, B.M.; McKeown, N.B. Enhancing the rigidity of a network polymer of intrinsic microporosity by the combined use of phthalocyanine and triptycene components. *Polym. Chem.* **2011**, *2*, 2190–2193. [[CrossRef](#)]
31. Ding, S.M.; Sun, L.; Ma, X.H.; Cheng, D.; Wu, S.H.; Zeng, R.; Deng, S.J.; Chen, C.; Zhang, N. Microporous polymeric spheres as highly efficient and metal-free catalyst for the cycloaddition of CO<sub>2</sub> to cyclic organic carbonates at ambient conditions. *Catal. Lett.* **2020**, *150*, 2970–2977. [[CrossRef](#)]
32. Jiang, Q.Q.; Wang, X.; Wu, Q.; Li, Y.J.; Luo, Q.X.; Mao, X.L.; Cai, Y.J.; Liu, X.; Liang, R.P.; Qiu, J.D. Rapid charge transfer enabled by noncovalent interaction through guest insertion in supercapacitors based on covalent organic frameworks. *Angew. Chem. Int. Ed.* **2023**, *62*, e202313970. [[CrossRef](#)]
33. Zhang, W.W.; Ping, R.; Lu, X.Y.; Shi, H.B.; Liu, F.S.; Ma, J.J.; Liu, M.S. Rational design of Lewis acid-base bifunctional nanoparticles with high performance on CO<sub>2</sub>/epoxide cycloaddition without a cocatalyst. *Chem. Eng. J.* **2023**, *451*, 138715–138724. [[CrossRef](#)]
34. Yan, T.; Liu, H.; Zeng, Z.X.; Pan, W.G. Recent progress of catalysts for synthesis of cyclic carbonates from CO<sub>2</sub> and epoxides. *J. CO<sub>2</sub> Util.* **2023**, *68*, 102355–102370. [[CrossRef](#)]
35. Nyokong, T. Coord. Effects of substituents on the photochemical and photophysical properties of main group metal phthalocyanines. *Coord. Chem. Rev.* **2007**, *251*, 1707–1722. [[CrossRef](#)]
36. Canlica, M.; Booyesen, I.N.; Nyokong, T. Syntheses, electrochemical and spectroelectrochemical properties of novel ball-type and mononuclear Co(II) phthalocyanines substituted at the peripheral and non-peripheral positions with binaphthol groups. *Polyhedron* **2011**, *30*, 508–514. [[CrossRef](#)]
37. Wagh, G.D.; Akamanchi, K.G. Sulfated tungstate catalyzed synthesis of C<sub>3</sub>-symmetric 1,3,5-triaryl benzenes under solvent-free condition. *Tetrahedron Lett.* **2017**, *58*, 3032–3036. [[CrossRef](#)]
38. Sakamoto, K.; Ohno, E. Synthesis of cobalt phthalocyanine derivatives and their cyclic voltammograms. *Dye. Pigment.* **1997**, *35*, 375–386. [[CrossRef](#)]
39. Achar, B.N.; Lokesh, K.S. Studies on polymorphic modifications of copper phthalocyanine. *J. Solid State Chem.* **2004**, *177*, 1987–1993. [[CrossRef](#)]
40. Zhang, T.; Wang, X.F.; Huang, X.L.; Liao, Y.N.; Chen, J.Z. Bifunctional catalyst of a metallophthalocyanine-carbon nitride hybrid for chemical fixation of CO<sub>2</sub> to cyclic carbonate. *RSC Adv.* **2016**, *6*, 2810–2818. [[CrossRef](#)]
41. Rabchinskii, M.K.; Ryzhkov, S.A.; Besedina, N.A.; Brzhezinskaya, M.; Malkov, M.N.; Stolyarova, D.y.; Arutyunyan, A.F.; Struchkov, N.S.; Saveliev, S.D.; Diankin, I.D.; et al. Guiding graphene derivatization for covalent immobilization of aptamers. *Carbon* **2022**, *196*, 264–279. [[CrossRef](#)]
42. Tahir, H.B.; Abdullah, R.M.; Aziz, S.B. The H<sup>+</sup> ion transport study in polymer blends incorporated with ammonium nitrate: XRD, FTIR, and electrical characteristics. *Results Phys.* **2022**, *42*, 105960. [[CrossRef](#)]
43. Zhang, Z.; Dou, M.; Liu, H.; Dai, L.M.; Wang, F. A facile route to bimetal and nitrogen-codoped 3D porous graphitic carbon networks for efficient oxygen reduction. *Small* **2016**, *12*, 4193–4199. [[CrossRef](#)]
44. Samal, P.P.; Deshshinamoorthy, A.; Arunachalam, S.; Vijayaraghavan, S.; Krishnamurthy, S. Free base phthalocyanine coating as a superior corrosion inhibitor for copper surfaces: A combined experimental and theoretical study. *Colloids Surf. A Physicochem. Eng. Asp.* **2022**, *648*, 129138. [[CrossRef](#)]
45. Ivanco, J.; Toader, T.; Firsov, A.; Brzhezinskaya, M.; Sperling, M.; Braun, W.; Zaha, D.R.Z. Indium on a copper phthalocyanine thin film: Not a reactive system. *Phys. Rev. B* **2010**, *81*, 115325. [[CrossRef](#)]
46. Shmatko, V.A.; Yalovega, G.E.; Myasiedova, T.N.; Brzhezinskaya, M.M.; Shtekhin, I.E.; Petrov, V.V. Influence of the surface morphology and structure on the gas-sorption properties of SiO<sub>2</sub>CuO<sub>x</sub> nanocomposite materials: X-ray spectroscopy investigations. *Phys. Solid State* **2015**, *57*, 399. [[CrossRef](#)]

47. Yalovega, G.E.; Myasoedova, T.N.; Shmatko, V.A.; Brzhezinskaya, M.M.; Popv, Y.V. Influence of Cu/Sn mixture on the shape and structure of crystallites in copper-containing films: Morphological and X-ray spectroscopy studies. *Appl. Surf. Sci.* **2016**, *372*, 93–99. [[CrossRef](#)]
48. Saptal, V.; Shinde, D.B.; Banerjee, R.; Bhanage, B.M. State-of-the-art catechol porphyrin COF catalyst for chemical fixation of carbon dioxide via cyclic carbonates and oxazolidinones. *Catal. Sci. Technol.* **2016**, *6*, 6152–6158. [[CrossRef](#)]
49. Guo, D.; Zhang, J.; Liu, G.; Luo, X.; Wu, F. Cobalt phthalocyanine-based nanodots as efficient catalysts for chemical conversion of CO<sub>2</sub> under ambient conditions. *J. Mater. Sci.* **2021**, *56*, 10990–10999. [[CrossRef](#)]
50. Xie, Y.; Wang, T.; Liu, X.; Zou, K.; Deng, W. Capture and conversion of CO<sub>2</sub> at ambient conditions by a conjugated microporous polymer. *Nat. Commun.* **2013**, *4*, 1960. [[CrossRef](#)]
51. He, L.; Natha, J.K.; Lin, Q. Robust multivariate metal-porphyrin frameworks for efficient ambient fixation of CO<sub>2</sub> to cyclic carbonates. *Chem. Commun.* **2019**, *55*, 412–415. [[CrossRef](#)] [[PubMed](#)]
52. Zheng, J.; Wu, M.Y.; Jiang, F.L.; Su, W.P.; Hong, M.C. Stable porphyrin Zr and Hf metal–organic frameworks featuring 2.5 nm cages: High surface areas, SCSC transformations and catalyses. *Chem. Sci.* **2015**, *6*, 3466–3470. [[CrossRef](#)] [[PubMed](#)]
53. Gao, W.Y.; Wojtas, L.; Ma, S.Q. A porous metal–metalloporphyrin framework featuring high-density active sites for chemical fixation of CO<sub>2</sub> under ambient conditions. *Chem. Commun.* **2014**, *50*, 5316–5318. [[CrossRef](#)]
54. Gao, W.Y.; Chen, Y.; Niu, Y.H.; Williams, K.; Cash, L.; Perez, P.J.; Wójcisz, L.; Cai, J.F.; Chen, Y.S.; Ma, S.Q. Crystal engineering of an nbo topology metal–organic framework for chemical fixation of CO<sub>2</sub> under ambient conditions. *Angew. Chem.* **2014**, *53*, 2615–2619. [[CrossRef](#)]
55. Ji, D.F.; Lu, X.B.; He, R. Syntheses of cyclic carbonates from carbon dioxide and epoxides with metal phthalocyanines as catalyst. *Appl. Catal. A Gen.* **2000**, *203*, 329–333. [[CrossRef](#)]
56. Sun, Q.; Aguila, B.; Perman, J.; Nguyen, N.; Ma, S.Q. Flexibility matters: Cooperative active sites in covalent organic framework and threaded ionic polymer. *J. Am. Chem. Soc.* **2016**, *138*, 15790–15796. [[CrossRef](#)]
57. Martín, C.; Fiorani, G.; Kleij, A.W. Recent advances in the catalytic preparation of cyclic organic carbonates. *ACS Catal.* **2015**, *5*, 1353–1370. [[CrossRef](#)]
58. Liang, J.; Huang, Y.B.; Cao, R. Metal–organic frameworks and porous organic polymers for sustainable fixation of carbon dioxide into cyclic carbonates. *Coord. Chem. Rev.* **2019**, *378*, 32–65. [[CrossRef](#)]
59. Wang, J.Q.; Kun, D.; Cheng, W.G.; Sun, J.; Zhang, S.J. Insights into quaternary ammonium salts-catalyzed fixation carbon dioxide with epoxides. *Catal. Sci. Technol.* **2012**, *2*, 1480–1484. [[CrossRef](#)]
60. Lan, J.W.; Qu, Y.; Ping, X.; Sun, J.M. Novel HBD-Containing Zn (dobdc) (datz) as efficiently heterogeneous catalyst for CO<sub>2</sub> chemical conversion under mild conditions. *Green Energy Environ.* **2021**, *6*, 66–74. [[CrossRef](#)]

**Disclaimer/Publisher’s Note:** The statements, opinions and data contained in all publications are solely those of the individual author(s) and contributor(s) and not of MDPI and/or the editor(s). MDPI and/or the editor(s) disclaim responsibility for any injury to people or property resulting from any ideas, methods, instructions or products referred to in the content.